

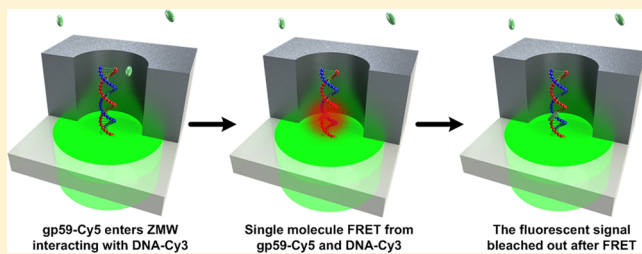
Dark-Field Illumination on Zero-Mode Waveguide/Microfluidic Hybrid Chip Reveals T4 Replisomal Protein Interactions

Yanhui Zhao,^{†,§} Danqi Chen,^{‡,§} Hongjun Yue,[‡] Michelle M. Spiering,[‡] Chenglong Zhao,[†] Stephen J. Benkovic,^{‡,*} and Tony Jun Huang^{*,†}

[†]Department of Engineering Science and Mechanics and [‡]Department of Chemistry, The Pennsylvania State University, University Park, Pennsylvania 16802, United States

Supporting Information

ABSTRACT: The ability of zero-mode waveguides (ZMWs) to guide light energy into subwavelength-diameter cylindrical nanoapertures has been exploited for single-molecule fluorescence studies of biomolecules at micromolar concentrations, the typical dissociation constants for biomolecular interactions. Although epi-fluorescence microscopy is now adopted for ZMW-based imaging as an alternative to the commercialized ZMW imaging platform, its suitability and performance awaits rigorous examination. Here, we present conical lens-based dark-field fluorescence microscopy in combination with a ZMW/microfluidic chip for single-molecule fluorescence imaging. We demonstrate that compared to epi-illumination, the dark-field configuration displayed diminished background and noise and enhanced signal-to-noise ratios. This signal-to-noise ratio for imaging using the dark-field setup remains essentially unperturbed by the presence of background fluorescent molecules at micromolar concentration. Our design allowed single-molecule FRET studies that revealed weak DNA–protein and protein–protein interactions found with T4 replisomal proteins.



KEYWORDS: Zero-mode waveguide, single-molecule FRET, dark-field microscopy, nanofabrication, microfluidic chip, T4 DNA replisome

Single-molecule fluorescence microscopy is among the plethora of single-molecule techniques that have been devised to interrogate individual molecules and complexes at the molecular level.^{1–6} This imaging technique has shown the capacity to discover and quantify the lifetimes and movements of novel species obscured by ensemble averaging in a broad spectrum of biological systems.^{7–19} The pursuit of detailed behavior concerning biomolecules through single-molecule fluorescence imaging, however, encounters the impediment of spatial resolution (~ 250 nm in lateral) imposed by the wavelike diffraction of light.^{20–28} As a result, to maintain single-molecule resolution within the typical focal volume of an \sim attoliter (10^{-18} L) of diffraction-limited microscopy, the accessible concentration range of fluorescent species is restricted to nanomolar to subnanomolar, markedly lower than the typical micromolar dissociation constants of biomolecular interactions.^{3,29,30}

A common scheme to overcome this “concentration barrier” in single-molecule fluorescence imaging is to have the fluorescently labeled biomolecules at their optimal concentrations but to excite only a limited number of molecules in the pool within the focal volume and have the majority of molecules unexcited.²⁹ This can be achieved by (1) stochastic activation of photoactivatable/switchable fluorophores, as in the case of STORM/PALM-type super-resolution microscopy and the photoactivation, diffusion, and excitation (PhADE)

approach;^{31–34} and (2) decreasing the focal volume in fluorescence imaging,^{35,36} as in the case of total internal reflection microscopy, confocal, and stimulated emission depletion microscopies, and zero-mode waveguides (ZMWs).^{37–46}

In particular, ZMW technology is an attractive platform for single-molecule imaging due to the high parallelism and most importantly, to its tolerance of high concentrations of fluorescent species.^{47–50} ZMWs, the subwavelength-diameter cylindrical nanoapertures clad in metal (e.g., aluminum) (Figure 1A), guide the incident excitation beam in a nonpropagating “zero mode” to form an evanescent excitation field at the entrance of the cylinder with a typical observation volume of \sim zeptoliter (10^{-21} L) (Figure 1B), a volume \sim 3 orders of magnitude smaller than that in diffraction-limited microscopy. Because of this superior optical confinement property, single-molecule fluorescence imaging using a ZMW allows for the detection of single excited fluorescently labeled biomolecules despite the presence of up to $10\ \mu\text{M}$ out-of-focus background fluorescent species.

Since its inception, this nanostructure has found ample utility in single-molecule investigations of a growing list of biological

Received: December 27, 2013

Revised: February 24, 2014

Published: March 14, 2014

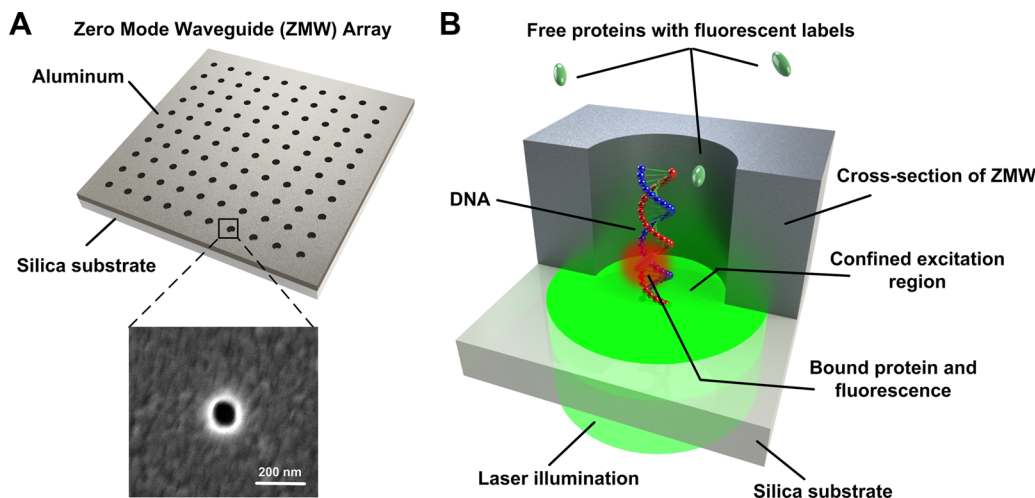


Figure 1. (A) Schematic of a zero-mode waveguide (ZMW) array. Typical ZMWs are subwavelength-diameter cylindrical nanowells in ~100 nm thick aluminum coated on top of a silica substrate. The magnified square region shows the SEM image of the 90 nm diameter ZMW used throughout this study. (B) The optical confinement property of a ZMW for single-molecule fluorescence studies. As light (i.e., 532 nm green laser) penetrates into a 50–100 nm diameter ZMW from the silica side, its intensity exponentially attenuates to generate an evanescent excitation field of ~zeptoliters (10^{-21} L). This optical property allows for single-molecule fluorescence studies of biomolecular interactions (i.e., interactions between ZMW-immobilized DNA and a DNA-interacting protein in bulk solution) to be carried out in ZMWs at micromolar (μ M) bulk concentrations of fluorescent biomolecules.

targets.^{51–57} The accessibility of a ZMW-based single-molecule fluorescence platform, however, remains limited to a handful of specialized laboratories due to the stringent technical requirements in nanofabrication, surface passivation, and microscopy instrumentation.^{58,59} Although these constraints have recently been relieved somewhat as more efforts have been directed to the optimization of ZMW nanofabrication protocols and the development of surface passivation methods, the simplification of a single-molecule fluorescence microscopy setup for ZMWs and the optimization of its performance have remained challenging. Holographic confocal fluorescence microscopy in which sophisticated optics are employed in complex light paths to generate thousands of subillumination spots and corresponding prism-dispersed emission spots that match the pattern of ZMW arrays was originally developed for ZMW-based single-molecule imaging.⁶⁰ The level of complexity and the costly investment of this microscopy setup are not amenable to its widespread implementation, despite its superior performance. Alternatively, epi-fluorescence microscopy (Epi) was implemented in ZMW-based fluorescence imaging;⁵² however, this microscopy setup is not tailored for illuminating ZMWs and the performance of Epi to image single fluorophores residing in the highly reflective aluminum clad ZMWs (Al/ZMWs) has not been rigorously investigated. In short, a simple, optimized microscope setup would facilitate the generalization of the ZMW-based single-molecule imaging technique.

In this study, we developed a conical lens-based dark-field fluorescence microscope tailored for ZMW illumination. Through side-by-side comparison with Epi, we found that the dark-field setup effectively decreased the background fluorescence and noise levels by alleviating the leakage of ZMW surface reflected illumination into the fluorescence detection module. In single-molecule photobleaching measurements with Al/ZMWs, the dark-field setup has an average signal-to-noise ratio (S/N) of 5.13 compared to 1.78 for the Epi setup. This substantial improvement in imaging performance permitted ZMW-based single-molecule FRET studies at micromolar background fluorophore concentrations without substantial

deterioration of the S/N ratio. This in turn enabled real-time investigation of a weak single-stranded DNA (ssDNA)-protein interaction and a rare protein–protein interaction within the T4 replisome.

Results and Discussion. The accessibility of a high-performance, single-molecule fluorescence microscope for ZMW-based imaging has constrained the widespread implementation of this technology in biological studies. On one hand, dissemination of this method has been hampered by the complexity and high cost associated with the multiplexed confocal microscopy designed for ZMW in which a collimated laser beam is holographically split into thousands of sub-beams, each one designated to a specific ZMW. On the other hand, an alternative Epi setup was employed for illuminating the highly reflective Al/ZMWs, which taxed the efficiency of conventional Epi to filter the potentially strong reflected excitation beam from the fluorescence signal. We have demonstrated a proof-of-concept ZMW/microfluidic hybrid chip as a prototype for a future ZMW-based, on-chip single-molecule imaging platform. We also improved the detection sensitivity of our single-molecule platform through signal-to-noise ratio enhancement from our customized optical design.

Conical Lens-Based Dark-Field Illumination on a ZMW/Microfluidic Hybrid Chip. The working mode of a ZMW demands that both the incident illumination laser and the signal collection be carried out from the coverslip side of ZMW arrays through an objective lens causing the reflected incident laser light to overlap with the weak backscattering fluorescent signals. To avoid signal deterioration, a proper dichroic filter is often installed in conventional microscopy to selectively collect the fluorescent emissions and block the unwanted reflected excitation beam. When Al/ZMWs are illuminated in the Epi mode, the strong reflected illumination beam caused by the smooth, highly reflective Al film surface imposes high demands on the dichroic filter for complete reflection blocking. Unlike the Epi configuration, a multiplexed confocal microscope sidesteps the interference from the reflected excitation beam by generating a patterned illumination composed of numerous

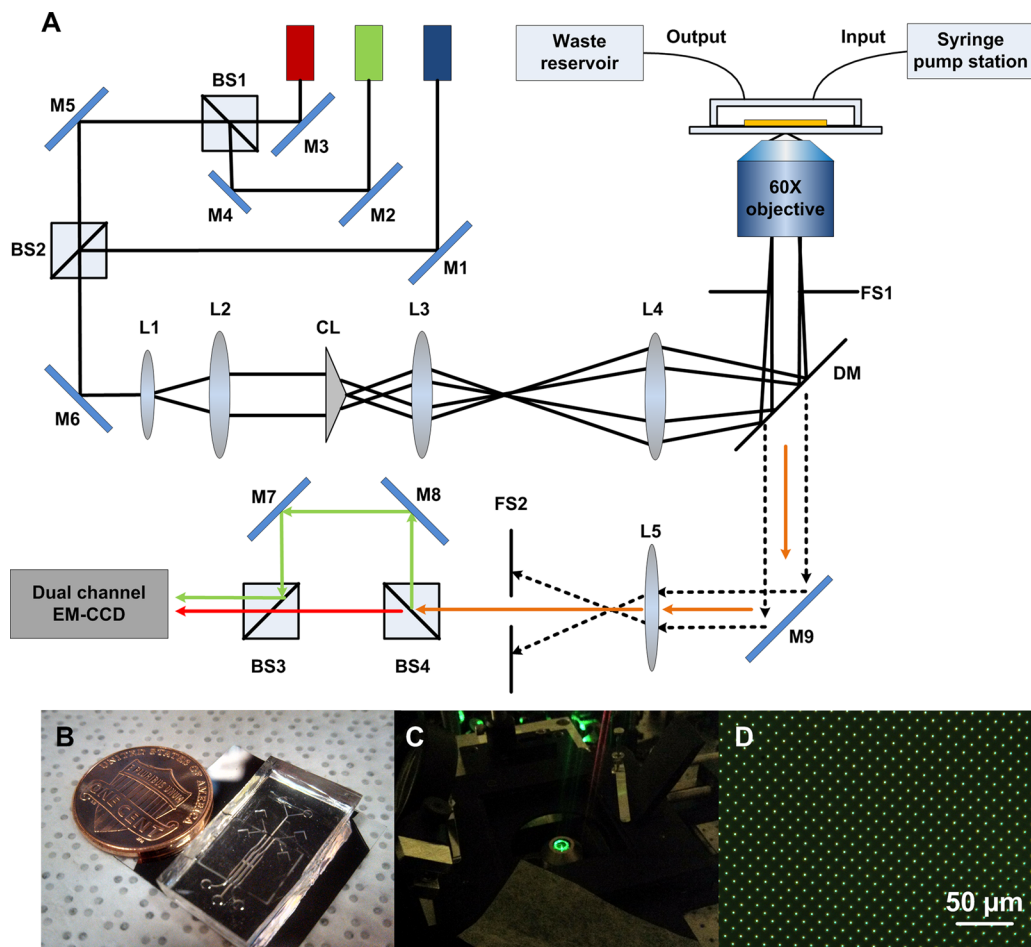


Figure 2. Conical lens-based dark-field microscopy in combination with ZMW/microfluidic chip for single-molecule imaging. (A) The microscope setup was built on an inverted microscope. The 532 nm (green), 635 nm (red), and 488 nm (blue) lasers were superimposed by mirrors (M1–M6) and beam splitters (BS1, BS2). The merged beams were then expanded by lenses (L1 and L2) and rendered into a doughnut shape by a conical lens (CL). Lenses L3 and L4, together with a dichromic mirror (DM) and a field stopper (FS1), directed the beams to focus at the back focal point of a water-immersion 60× objective. Placed on top of the objective, the ZMW/microfluidic channel connected with a syringe pump acted as a sealed reaction chamber. Fluorescence emission signals (orange arrow) from Cy3 and Cy5 dyes collected through the objective were split by BS3, BS4, M7, and M8 for the dual-channel EMCCD detection. Any peripheral reflected excitation beams (dotted line), which leaked into the detection module, were removed by FS2. (B) ZMW/microfluidic chip for single-molecule fluorescence measurements, (C) the doughnut-shape illumination beam (532 nm) rendered by the dark-field illumination configuration, and (D) optical image of a ZMW array.

split beams that pinpoint the silica bottom of the ZMWs.⁶⁰ However, this confocal microscope arrangement is technically challenging to implement.

We have attempted to address the issues with a simple yet effective conical lens-based dark-field fluorescence microscope. We point out that commercially available dark-field microscopes that work either by a transmission mode, as in the case of an inverted dark-field microscope, or rely on specially designed objective lenses, as in the case of an up-right dark-field microscope, are incompatible with the reflection mode required by ZMW imaging. We thus designed an inverted dark-field microscope that uses a reflection mode enabled by a conical lens. The instrument has a customized optical path depicted in Figure 2A, where the light from its three lasers is first superimposed by two beam splitters (BS1 and BS2) and then rendered by a conical lens (CL) and lenses L1 and L2 to a “doughnut” like beam with zero intensity at the center and maxima at the rim (Figure 2C). This light pattern is then tuned by lenses L3 and L4 to focus at the back focal plane of the 60× objective to illuminate the ZMW array. A detailed view of our setup and the superior dark-field image of 2.8 μm diameter

polystyrene beads that the setup enabled are given in Figure S2D in Supporting Information.

Our proposed design addresses the reflection issue in Al/ZMW imaging because it separates the backscattering fluorescence signal from the reflected, incident light. Given that the doughnut-shaped beam impinges on the ZMWs with a large incident angle through the 60× objective (NA = 1.2), any reflection from the metal interface would either escape by the same illumination pathway or be cut off by the aperture of the objective, thereby reducing any reflection that leaks into the center region of the objective lens. This then essentially separates the optical path of the desired fluorescence signal from that of the incident and reflected beams as the fluorescent signal (orange arrow, Figure 2A), collected by the objective lens, localizes in the center region that is largely orthogonal to both the incident and reflected excitation located at the peripheral doughnut rim (dot line, Figure 2A).

We have also demonstrated an integration of ZMWs with a microfluidic system (Figure 2B) to take advantage of the high-precision fluidic control enabled by microfluidic techniques.^{61–63} Mounted on the microscope stage, a coverslip with

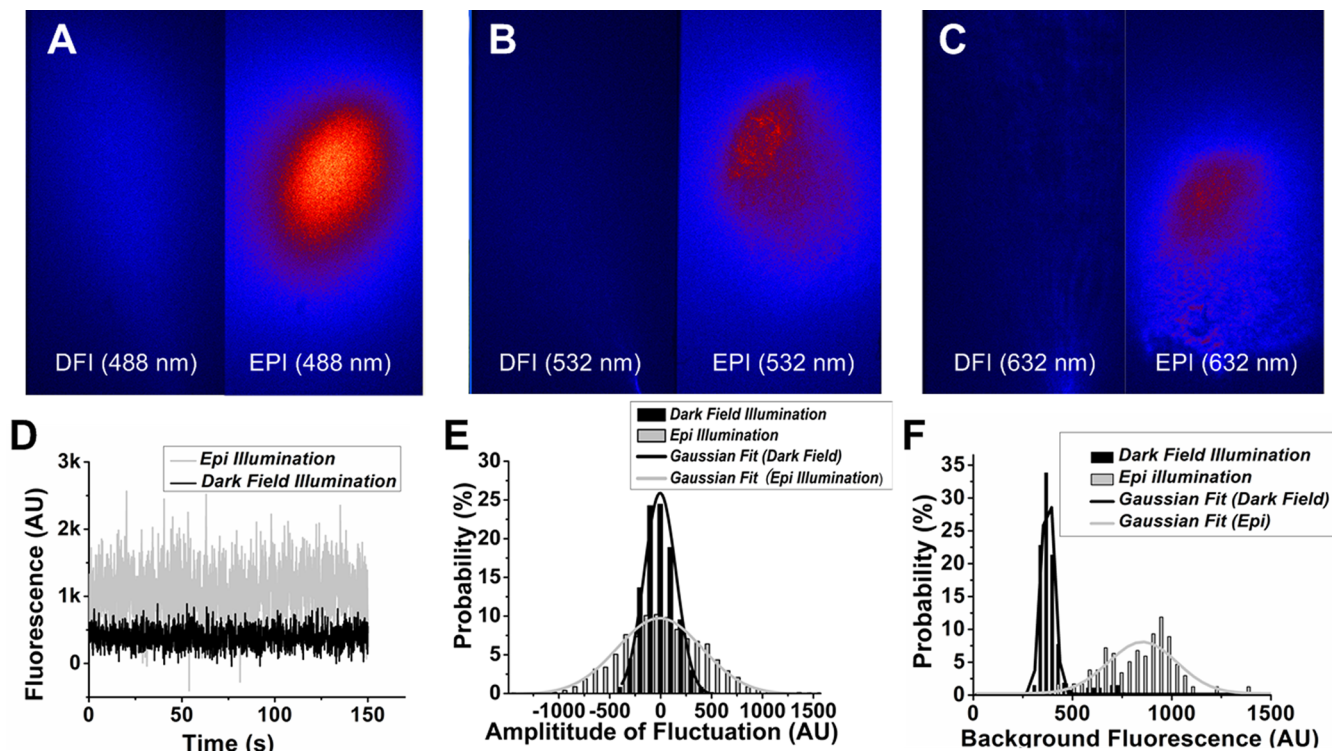


Figure 3. EMCCD images of the background fluorescence in emission detection channels for (A) Cy2, (B) Cy3, and (C) Cy5 for ZMWs in dark field (DFI, left panel) and Epi (EPI, right panel) configurations illuminated by the blue (488 nm), green (532 nm), and red (635 nm) lasers, respectively. The ZMWs were free of fluorescent molecules. The fluorescence intensity in the image was color-coded according to the spectral gradient from blue (intensity minimum) to red (intensity maximum). (D) A representative time trace for the background fluorescence in the Cy3 detection channel of ZMWs in Epi (gray) and dark field (black) configurations illuminated with the green (532 nm) laser. (E) Fluctuations of the background fluorescence of a representative time trace. The histograms were plotted using the data in (D) and were fit to a Gaussian function to give standard deviations for the noise level of 832 AU for Epi and 312 AU for dark-field. AU: arbitrary units. (F) Distribution of the background fluorescence intensity in the Cy3 detection channel of ZMWs in Epi (gray) and dark-field (black) configurations illuminated with the green (532 nm) laser. The mean background values from 250 fluorescence traces from either illumination configuration were plotted in histograms, which were fit to a Gaussian function to give the median background fluorescence levels of 853 ± 417 AU for Epi and 376 ± 61 AU for dark-field.

a 90 nm diameter ZMW array (Figure 2D) was integrated with a polydimethylsiloxane (PDMS) microfluidic channel and a syringe pump system to form a ZMW/microfluidic chip (Figure 2B) as a reaction chamber for single-molecule fluorescence imaging. The precise, uniform dimensions ($10 \text{ mm} \times 2 \text{ mm} \times 0.2 \text{ mm}$) of the microfluidic channels not only require very small volumes of the reaction mixture ($\sim 4 \mu\text{L}$), but they also permit deploying multiple microchannels in a $25 \times 25 \text{ mm}^2$ area with ZMWs for parallel reactions. Equipped with a syringe pump system, the ZMW/microfluidic chip was functionalized/passivated by sequentially injecting one at a time antidigoxigenin antibody (Anti-Dig), BSA, 5'-Dig-ssDNA primer labeled with Cy3, and dye-labeled fluorescent molecules with washes between each injection in a programmable fashion. In addition, the PDMS microfluidic molding served to seal the ZMW reactors helping to maintain the pH value of the reaction mixture by isolating the acid-producing antiphotobleaching oxygen scavenger system from ambient oxygen.

This proof-of-concept ZMW/microfluidic hybrid design benefits single-molecule experiments from the following aspects: (1) Microfluidics help to reduce the sample consumption of reagents that are difficult to obtain, such as human proteins. It can effectively deliver such reagents precisely to where the experiment will be monitored and significantly reduce the sample consumption. (2) The microfluidic systems can precisely control the reaction fluids in terms of reaction amount, volume, time, and so forth. The

microfluidic systems also help to ensure consistent reaction conditions for each experiment, increasing reproducibility for large quantities of data collection and analysis. (3) The microfluidic channels can effectively seal the reaction solutions inside the microfluidic channel, protecting and isolating the reactants and the reaction from the environment. (4) Using microfluidic systems, we are able to achieve numerous parallel reactions on one chip permitting automated high-throughput screening and analysis. A prototype of the integration of a microfluidic chip and a ZMW single-molecule detection platform is shown in Figure 2. All of our experiments are conducted using this lab-on-a-chip platform (also shown in Figure S2 in Supporting Information).

Background Noise Levels and Fluorescence of Epi and Dark-Field Fluorescence Microscopes. To evaluate the collection of the reflected incident excitation beam by Al/ZMW arrays in the conventional Epi and the conical lens-based dark-field microscope setups, we measured the background fluorescence and noise levels of the two setups using the three different colored lasers (488, 532, and 635 nm) to illuminate the Al/ZMW chip without any fluorescent molecule present. The incident lasers were set at 50% power output (measured $\sim 165 \text{ mW}$) with a proper dichroic filter installed for each laser to block the reflected excitation beam. As shown in the color-coded EMCCD images of ZMWs illuminated by the three lasers individually (Figure 3A–C), the background fluorescence of the Epi setup was substantially stronger than that of the dark-

field setup, most likely caused by the leakage of the strong reflected excitation beam despite the installation of the dichroic filter in the Epi setup. From representative time-resolved fluorescence traces for the fluorescence in the Cy3-detection channel of ZMWs illuminated with the green (532 nm) laser in both configurations (Figure 3D), we found that the background fluorescence levels (mean values, 1039 versus 363 in arbitrary units, AU), as well as the fluctuation of the background fluorescence levels defined as noise (832 vs 312 in AU) were substantially higher in the case of the Epi setup (Figure 3E). The distribution histograms of the background fluorescence levels based on the statistics of 250 traces obtained from both setups (Figure 3F) consistently showed that the dark-field setup has a lower average value (376 AU) than the Epi setup (853 AU) and a much narrower distribution of the background fluorescence fluctuations also.

Single-Molecule Photobleaching Measurements with ZMWs in the Presence/Absence of Fluorophores in Bulk. We have shown that the conical lens-based dark-field microscope suppresses the background fluorescence and noise levels as a result of the reduced collection of reflected excitation beams by the Al/ZMWs surface. We next set out to examine the impact of the reflected excitation beams on the performance of the dark-field and Epi setups in single-molecule fluorescence measurements with ZMW arrays using S/N from Cy3 as the criterion. First, we studied single-molecule fluorescence bleaching of Dig- and Cy3-labeled DNA primers immobilized in ZMWs. The 532 nm laser in either the Epi or dark-field mode excited the tethered primers until completely photobleached. The laser power was measured \sim 50 mW (measured at the objective) for all measurements. Noting that the power density calculated from measured illumination intensity over the illumination region may be different for each case, depending on the focusing condition and region; however, it is not a critical factor as the intensity is strong enough for fluorophore excitation in each experiment. The S/N ratio improvement has been achieved through splitting fluorescence and directing reflections away from our dark-field detection path. The Cy3 detection channel of the EMCCD-recorded images was used to identify fluorescent spots, which were then analyzed to generate time-resolved single-molecule fluorescence traces. As shown in Figure 4A, the first recorded color-coded EMCCD images of the Cy3 primers excited by Epi gave an overall blurred image of the ZMW array pattern due to the significantly higher background fluorescence. Accordingly, numerous false emitters in addition to the ones residing in ZMWs were recognized and lead to uninformative time traces. In marked contrast, the image from the dark-field setup displayed suppressed background fluorescence and a clear view of ZMW array containing excited Cy3 primers, which were identified as individual fluorophores with little or no false positives.

Figures 4B and 4C show examples of time-resolved fluorescence traces with single-step photobleaching events from the Epi and dark-field setups, respectively. Consistent with the reduced background fluorescence and noise, and the high S/N ratio of the dark-field arrangement in general, this configuration had an overall higher S/N ratio (5.13) compared to Epi (1.78) averaged from the measured ratios of \sim 250 photobleaching events in both cases (Figure 4D). In addition, the probability of a S/N ratio \geq 3, a criterion for unambiguous identification of single-molecule events in microscopy analysis,⁶⁴ was 85.3% for the dark-field setup and 22.4% for the Epi

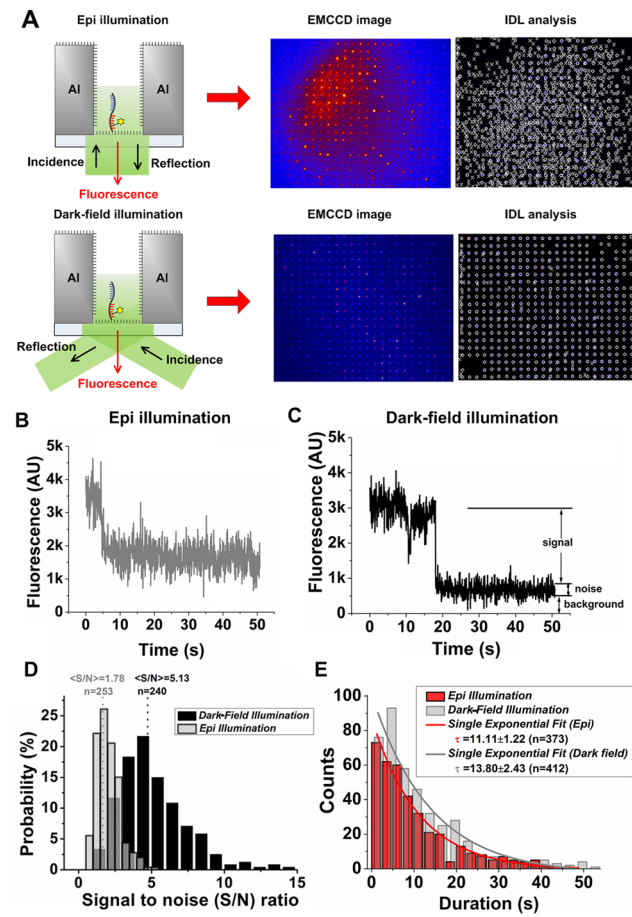


Figure 4. (A) Schematic of single-molecule photobleaching of the immobilized Cy3-DNA primer in a ZMW using the green (532 nm) laser in either the Epi or dark-field microscopy configurations. ZMWs were functionalized with antidigoxigenin antibody and then passivated with BSA. A Cy3-DNA primer was immobilized through a digoxigenin: antidigoxigenin antibody interaction. EMCCD images and IDL analysis results of the Cy3-primers immobilized in ZMW arrays excited by the 532 nm laser in the Epi or dark-field configuration are shown. Fluorescence intensity was color-coded according to the spectral gradient from blue (intensity minimum) to red (intensity maximum). AU indicates arbitrary units. Representative single-step photobleaching trajectories of the Cy3-DNA primer excited by the 532 nm green laser in the (B) Epi and (C) dark-field configurations. (D) Distribution of the signal-to-noise ratio (S/N) in the single-molecule photobleaching measurements using the Epi (gray) and the dark-field configurations (black). The S/N was calculated as described in the section of “Single Molecule Data Acquisition and Analysis” in the SI. Histograms were plotted using the S/N values from 240 (Epi) and 253 (dark-field) photobleaching events. The mean S/N ratios for the Epi and dark-field microscopies were 1.78 and 5.13, respectively. (E) Distribution of the fluorescence duration of the immobilized Cy3-DNA primers in single-molecule photobleaching measurements using the Epi (red) and dark-field (gray) configurations. Single-exponential fitting yielded the fluorescence durations (τ) of 11.11 ± 1.22 s ($n = 373$) for the Epi and 13.80 ± 2.43 s ($n = 412$) for dark-field setup.

setup. To warrant these S/N ratio comparisons, we tested the excitation/bleaching of the immobilized Cy3 primers in ZMWs under the same excitation intensity and statistically analyzed the fluorescence duration of \sim 400 photobleaching events using both setups (Figure 4E). Because of the near-linear relationship between fluorescence duration and excitation intensity, the

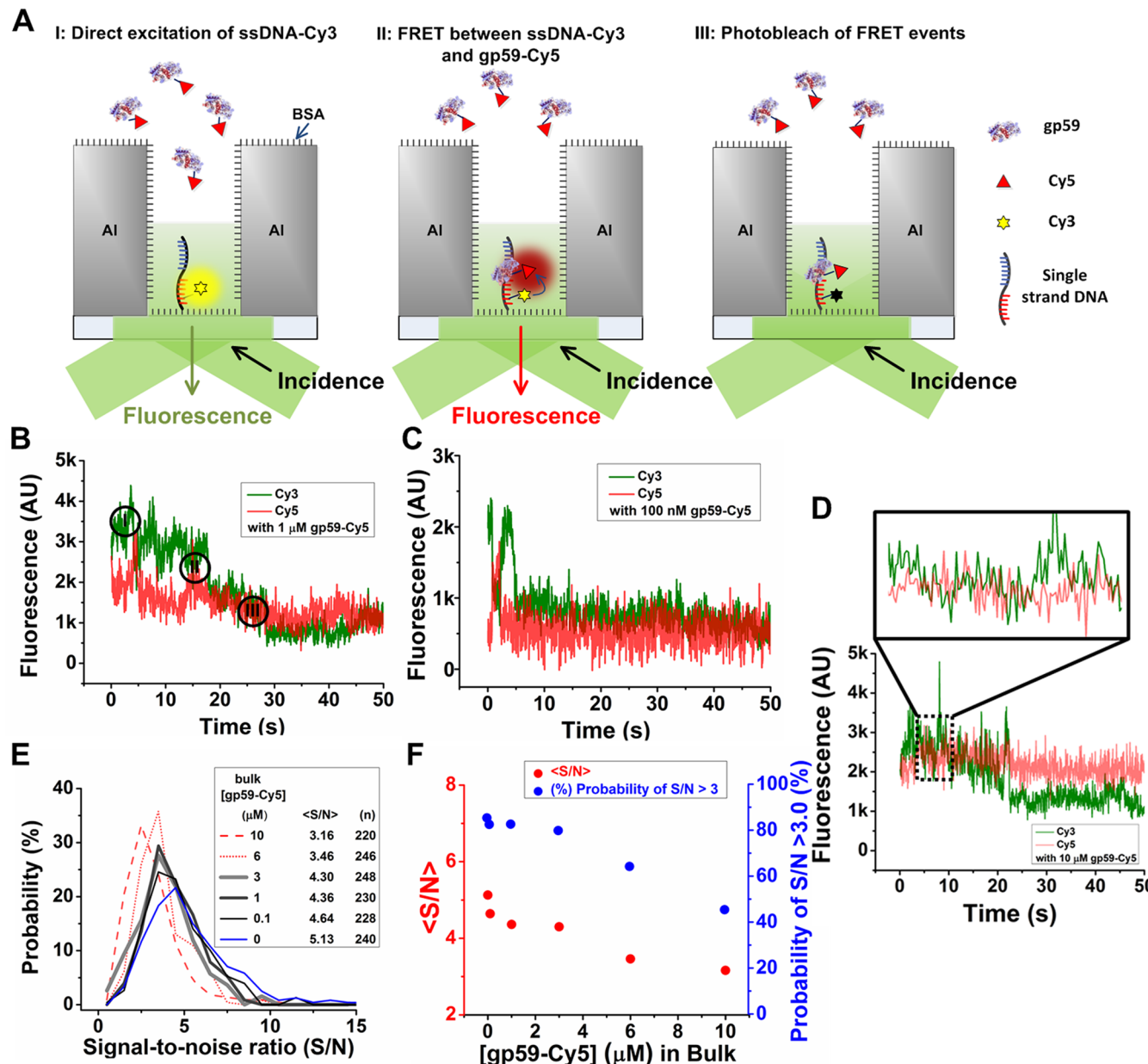


Figure 5. (A) Schematic of single-molecule photobleaching of the immobilized Cy3-DNA primer in ZMWs in the presence of bulk gp59(C42)-Cy5 excited by the green (532 nm) laser in the dark-field illumination configuration. Representative time traces of the single-molecule photobleaching of the Cy3-DNA primer in the presence of (B) 1 μ M, (C) 100 nM, and (D) 10 μ M gp59(C42)-Cy5. The fluorescence intensities of the Cy3 and Cy5 channels are in green and red, respectively. (E) Distribution of the S/N ratio in the single-molecule photobleaching measurements of the Cy3-DNA primer in the presence of 0 nM (blue), 100 nM (black), 1 μ M (dark gray), 3 μ M (gray), 6 μ M (red, dot line) and 10 μ M (red, dash line) gp59(C42)-Cy5. (F) Mean S/N ratios ($\langle S/N \rangle$) and probability of S/N ratio larger than 3 as a function of gp59(C42)-Cy5 concentration.

comparable characteristic duration time (τ) obtained by single-exponential fitting of the distribution plots (11.11 s (Epi) versus 13.80 s (dark-field)) proved that despite the different illumination modes, the two microscope arrangements generated excitation fields in the ZMW arrays with essentially equivalent intensities.⁶⁵

ZMWs are known as nanostructures in which single-molecule imaging can be carried out in the presence of micromolar bulk fluorophores. To test whether the dark-field configuration was successful with ZMWs at high concentrations of bulk fluorophores, we determined the S/N ratios again in similar single-molecule photobleaching measurements, but in the presence of up to 10 μ M Cy5-labeled gp59 (gp59(C42)-Cy5), the helicase loader protein in the T4 bacteriophage DNA

replisome (Figure 5A).^{66–69} Because gp59 is known to bind to single-stranded DNA, the representative fluorescence time trace of tethered Cy3-DNA primer in ZMWs in the presence of 100 nM or 1 μ M gp59(C42)-Cy5 displayed clear FRET events between the dyes on the DNA and gp59 before photobleaching of the Cy3 dye (Figures 5B,C).⁷⁰ In the case of 10 μ M bulk dye-labeled gp59, FRET events were less discernible in the representative time trace, owing to the increased level of cy5 emission (Figure 5D). The occurrence of FRET events was dependent on the gp59 concentration. As shown in Figure 5E, the overall S/N ratio distribution remained largely unperturbed by the presence of up to 3 μ M of background gp59(C42)-Cy5. A noticeable shift of the distribution curve occurred at 6 μ M gp59. The mean S/N ratio ($\langle S/N \rangle$) and probability of S/N

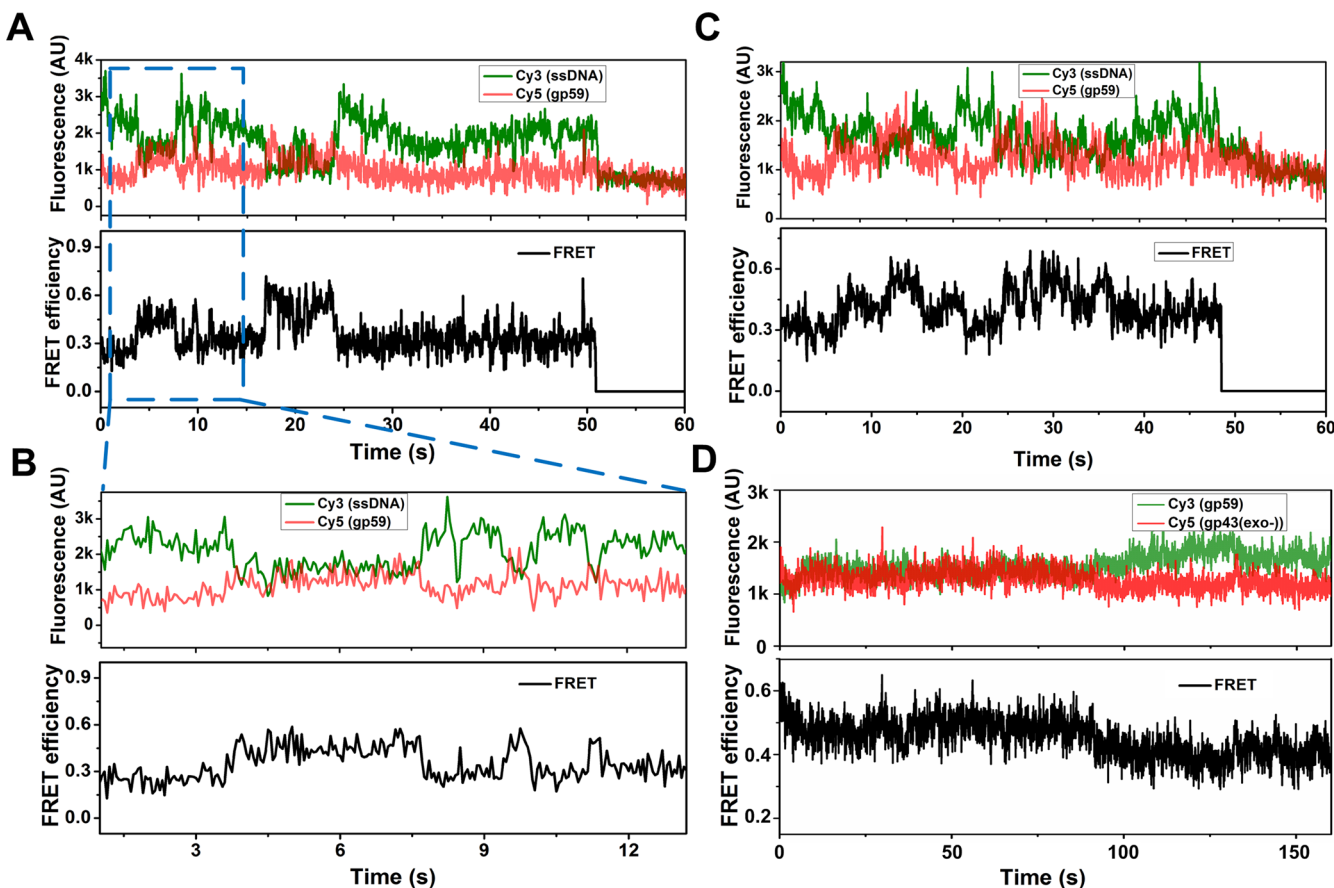


Figure 6. (A) Representative FRET and FRET efficiency trajectories for the interaction between the Cy3-ssDNA primer and gp59(C42)-Cy5 in a ZMW. gp59(C42)-Cy5 was at 1 μM bulk concentration. The fluorescence intensities of the Cy3 and Cy5 emissions are in green and red, respectively. (B) A magnified view of the FRET events and their FRET efficiency in the square region of (A). (C) FRET and FRET efficiency time trajectories show the presence of three major FRET states with apparent FRET efficiencies of 0.37, 0.45, and 0.6. (D) Representative FRET and FRET efficiency time trajectories between the gp59(C42)-Cy3 and Cy5-N-gp43(exo-) on the immobilized DNA primer in a ZMW.

larger or equal to 3 (% ($S/N > 3$)) remained constant at ~ 4.5 and 80% at less than 3 μM gp59. The deterioration of the two parameters was displayed when gp59 was greater than 6 μM . At 10 μM gp59, $\langle S/N \rangle$ decreased to 3.16 and % ($S/N > 3$) to 45%. In order to find out why the S/N ratio decreased as fluorophore concentration increased, we measured the background fluorescence level in the Cy3 emission channel for ZMWs with up to 8 μM bulk Cy5-labeled gp59. A ZMW chip, free of surface immobilized Cy5-fluorophores, was illuminated with the 532 nm laser. In good agreement with the above S/N changes, mean background fluorescence and the breadth of the distribution showed a substantial increase in the range of 4–6 μM bulk gp59 concentration (Supporting Information Figure S3J,K). Thus, the decrease in S/N ratio at $>6 \mu\text{M}$ bulk fluorophore originated from the deterioration of the background fluorescence. We attributed this to the increased nonspecific binding of the protein on ZMW surfaces at higher concentrations and the relatively high focal volume of our dark-field setup. In light of these findings, we conclude that conical lens-based dark-field microscopy achieves a substantial improvement in the S/N ratio in ZMW single-molecule imaging by alleviating the interference of the Al/ZMW surface-reflected excitation beam. Moreover, the optimal background fluorophore concentration range of 0–4 μM is comparable to the previously reported range (up to 10 μM) of the commercialized ZMW imaging platform. These advantages,

as well as the ease of implementation, make the dark-field microscope a more reliable alternative to the Epi setup, and a more implementable alternative to the commercialized one for ZMW-based imaging.

ZMW/Single-Molecule FRET between DNA-Protein and Protein-Protein among the T4 Replisomal Proteins. The T4 DNA replication model system duplicates large DNA substrates at a rate of 400 bp/s by precisely orchestrating the complex interactions among the eight component proteins.^{66,71} This multiprotein complex has been a fertile ground for the practice of single-molecule fluorescence techniques, particularly single-molecule fluorescence resonance energy transfer (smFRET) by total internal reflection fluorescence microscopy (TIRFM) for unveiling dynamic behaviors of the interacting proteins within the T4 replisome.^{72–74} The concentration barrier of TIRFM, however, prevents single-molecule fluorescence studies on the T4 proteins at their physiological concentrations of sub-micromolar to micromolar.⁷⁴ We demonstrate here that a conical lens-based dark-field microscope in combination with the ZMW/microfluidic chip is positioned to remove this obstacle in single-molecule dynamic studies on the T4 replisomes.

We focused on one of the T4 proteins, gp59. Known as the helicase loader, gp59 also plays additional roles in homologous recombination, DNA repair, and initiation of DNA replication.^{74–77} Furthermore, it has remained elusive whether this

protein acts as an integral component in the T4 replisome post DNA replisome assembly. We first studied smFRET between the immobilized Cy3-ssDNA primer in ZMWs and gp59(C42)-Cy5 in bulk. Previous ensemble studies showed that gp59 binds to a short ssDNA weakly with submicromolar binding affinity in multiple proposed binding modes.⁷⁰ Using the ZMW/dark-field microscope, we carried out experiments with 1 μM gp59 enabling single-molecule imaging at an adequate concentration for its interaction with the short ssDNA. We observed smFRET events and determined the FRET efficiency of each event (Figure 6A). In addition, consistent with the proposed binding modes, we found that there were three main FRET states as indicated by populations with apparent FRET efficiencies of 0.37, 0.45, and 0.60 (Figure 6B,C).

The real-time monitoring opened a new avenue of investigation into the kinetic characterization of the FRET states (binding modes) of gp59 on ssDNA, which would enormously contribute to the understanding of helicase loading by gp59. Through various ensemble investigations,^{69,78} it has been proposed that in the absence of the gp32 single-stranded DNA binding protein, gp59 through its interactions with DNA substrates recruits and orients the helicase on a DNA as a hexameric assembly. Thus, a description of the dynamics of gp59 interacting with DNA is integral to a comprehensive knowledge of the assembly process. The identification of the three main FRET states of gp59 on ssDNA by single-molecule imaging at physiological concentrations using our developed platform could be construed as an initial step to this end. Further characterization of the states is in progress.

In addition to the interaction with DNA, gp59 is also known to interact with other T4 replisomal proteins, including the gp43 polymerase, the gp32 single-stranded DNA-binding protein, the gp61 primase, and the gp41 helicase on DNA substrates, implicating its multiple roles in replication.^{69,76,79} We next attempted to study the dynamic interaction between gp59(C42)-Cy3 and Cy5-N-gp43(exo-) on the tethered ssDNA primer in ZMWs. Note that the interaction between gp59 and gp43 occurs preferably on forked-DNA substrates and that there is no report of such interaction on a short ssDNA primer.⁷⁹ Figure 6D shows a long (>80 s), rare FRET event between gp59 and gp43 on short ssDNA that was previously obscured in ensemble studies. As exemplified by this FRET study of a protein pair, our ZMW/dark-field single-molecule fluorescence microscope is poised to reveal a comprehensive kinetic picture of the interaction network involving gp59 and other proteins, and its functional relevance to the replication activity of the T4 replisome.

Conclusion. In this work, we aimed at addressing the constraints of the microscope configuration associated with the Al/ZMW nanostructures for single-molecule fluorescence imaging. With the advantages of simple optical deployment and effective suppression of the background fluorescence and noise levels by spatially separating the light path of the fluorescence emissions from the reflected excitation beam, the conical lens-based dark-field fluorescence microscope we employed has allowed single-molecule fluorescence measurements with high S/N ratios. We also showed that this microscopy setup in combination with the ZMW/microfluidic chip enabled smFRET studies on the weak interaction between a DNA primer (Cy3) and gp59 (Cy5) at up to micromolar concentrations, and rare binding events between gp59 (Cy3) and gp43 (Cy5) on a short DNA primer. This strongly suggests that this simple single-molecule instrument can be extended to

study the dynamic interactions that occur between the T4 replisomal proteins during the DNA replication process. Furthermore, we expect that this microscope will provide ample adaptability for add-on features extending the applications of ZMWs for single-molecule imaging studies on the T4 replisome. Particularly, integration of an alternating-laser excitation module for multicolor FRET or direct excitation using the multiple lasers would allow simultaneous imaging of the dynamic interactions of two or more differentially labeled T4 proteins at their physiological concentrations using ZMW arrays.

■ ASSOCIATED CONTENT

S Supporting Information

Y.Z., D.C., and H.Y. designed research and conducted experiment; Y.Z., D.C., and C.Z. built dark-field illumination setup; D.C. Y.Z., and M.M.S. analyzed the data and drafted manuscript, T.J.H. and S.J.B. oversaw the whole project. This material is available free of charge via the Internet at <http://pubs.acs.org>.

■ AUTHOR INFORMATION

Corresponding Authors

*E-mail: (S.L.B.) sjb1@psu.edu.

*E-mail: (T.J.H.) junhuang@psu.edu.

Author Contributions

[§]Y.Z. and D.C. are equal contribution authors.

Notes

The authors declare no competing financial interest.

■ ACKNOWLEDGMENTS

This work was supported by National Institutes of Health (NIH) Director's New Innovator Award 1DP2OD007209-01 (to T.J.H) and Grant GM013306 (to S.J.B.)

■ REFERENCES

- (1) Johnson, P. B.; Christy, R. W. *Phys. Rev. B* **1972**, 6 (12), 4370–4379.
- (2) Lu, H. P.; Xun, L.; Xie, X. S. *Science* **1998**, 282 (5395), 1877–82.
- (3) van Oijen, A. M. *Curr. Opin. Biotechnol.* **2011**, 22 (1), 75–80.
- (4) Forth, S.; Sheinin, M. Y.; Inman, J.; Wang, M. D. *Annu. Rev. Biophys.* **2013**, 42, 583–604.
- (5) Bai, L.; Santangelo, T. J.; Wang, M. D. *Annu. Rev. Biophys. Biomol. Struct.* **2006**, 35, 343–60.
- (6) Hilario, J.; Kowalczykowski, S. C. *Curr. Opin. Chem. Biol.* **2010**, 14 (1), 15–22.
- (7) Joo, C.; Balci, H.; Ishitsuka, Y.; Buranachai, C.; Ha, T. *Annu. Rev. Biochem.* **2008**, 77, 51–76.
- (8) Funatsu, T.; Harada, Y.; Tokunaga, M.; Saito, K.; Yanagida, T. *Nature* **1995**, 374 (6522), 555–9.
- (9) Giepmans, B. N.; Adams, S. R.; Ellisman, M. H.; Tsien, R. Y. *Science* **2006**, 312 (5771), 217–24.
- (10) Zhuang, X.; Bartley, L. E.; Babcock, H. P.; Russell, R.; Ha, T.; Herschlag, D.; Chu, S. *Science* **2000**, 288 (5473), 2048–51.
- (11) Ha, T. *Methods* **2001**, 25 (1), 78–86.
- (12) Min, W.; English, B. P.; Luo, G.; Cherayil, B. J.; Kou, S. C.; Xie, X. S. *Acc. Chem. Res.* **2005**, 38 (12), 923–31.
- (13) Finkelstein, I. J.; Greene, E. C. *Annu. Rev. Biophys.* **2013**, 42, 241–63.
- (14) Finkelstein, I. J.; Visnapuu, M. L.; Greene, E. C. *Nature* **2010**, 468 (7326), 983–7.
- (15) Gorman, J.; Greene, E. C. *Nat. Struct. Mol. Biol.* **2008**, 15 (8), 768–74.
- (16) Ha, T. *Cell* **2013**, 154 (4), 723–6.

- (17) Ha, T.; Kozlov, A. G.; Lohman, T. M. *Annu Rev Biophys* **2012**, *41*, 295–319.
- (18) Ha, T.; Tinnefeld, P. *Annu. Rev. Phys. Chem.* **2012**, *63*, 595–617.
- (19) Roy, R.; Hohng, S.; Ha, T. *Nat Methods* **2008**, *5* (6), 507–16.
- (20) Huang, B.; Bates, M.; Zhuang, X. *Annu. Rev. Biochem.* **2009**, *78*, 993–1016.
- (21) Fernandez-Suarez, M.; Ting, A. Y. *Nat Rev Mol Cell Biol* **2008**, *9* (12), 929–43.
- (22) Hell, S. W.; Dyba, M.; Jakobs, S. *Curr. Opin. Neurobiol.* **2004**, *14* (5), 599–609.
- (23) Klar, T. A.; Hell, S. W. *Opt. Lett.* **1999**, *24* (14), 954.
- (24) Zhang, X.; Liu, Z. *Nat. Mater.* **2008**, *7* (6), 435–41.
- (25) Liu, Z.; Lee, H.; Xiong, Y.; Sun, C.; Zhang, X. *Science* **2007**, *315* (5819), 1686.
- (26) Lu, D.; Liu, Z. *Nat. Commun.* **2012**, *3*, 1205.
- (27) Rho, J.; Ye, Z.; Xiong, Y.; Yin, X.; Liu, Z.; Choi, H.; Bartal, G.; Zhang, X. *Nat. Commun.* **2010**, *1*, 143.
- (28) Wei, F.; Liu, Z. *Nano Lett.* **2010**, *10* (7), 2531–6.
- (29) Zhu, P.; Craighead, H. G. *Annu. Rev. Biophys.* **2012**, *41*, 269–93.
- (30) Moran-Mirabal, J. M.; Craighead, H. G. *Methods* **2008**, *46* (1), 11–7.
- (31) Huang, B.; Babcock, H.; Zhuang, X. *Cell* **2010**, *143* (7), 1047–58.
- (32) Huang, B.; Wang, W.; Bates, M.; Zhuang, X. *Science* **2008**, *319* (5864), 810–3.
- (33) Bates, M.; Huang, B.; Zhuang, X. *Curr. Opin. Chem. Biol.* **2008**, *12* (5), 505–14.
- (34) Betzig, E.; Patterson, G. H.; Sougrat, R.; Lindwasser, O. W.; Olenych, S.; Bonifacino, J. S.; Davidson, M. W.; Lippincott-Schwartz, J.; Hess, H. F. *Science* **2006**, *313* (5793), 1642–5.
- (35) Zhao, Y.; Lin, S. C.; Nawaz, A. A.; Kiraly, B.; Hao, Q.; Liu, Y.; Huang, T. J. *Opt. Express* **2010**, *18* (22), 23458–65.
- (36) Zhao, C.; Liu, Y.; Zhao, Y.; Fang, N.; Huang, T. J. *Nat. Commun.* **2013**, *4*, 2305.
- (37) Tinnefeld, P. *Nat. Nanotechnol.* **2013**, *8* (7), 480–2.
- (38) Loveland, A. B.; Habuchi, S.; Walter, J. C.; van Oijen, A. M. *Nat. Methods* **2012**, *9* (10), 987–92.
- (39) Patterson, G.; Davidson, M.; Manley, S.; Lippincott-Schwartz, J. *Annu. Rev. Phys. Chem.* **2010**, *61*, 345–67.
- (40) Rust, M. J.; Bates, M.; Zhuang, X. *Nat. Methods* **2006**, *3* (10), 793–5.
- (41) Ji, N.; Shroff, H.; Zhong, H.; Betzig, E. *Curr. Opin. Neurobiol.* **2008**, *18* (6), 605–16.
- (42) Hell, S. W.; Wichmann, J. *Opt. Lett.* **1994**, *19* (11), 780.
- (43) Sahl, S. J.; Moerner, W. *Curr. Opin. Struct. Biol.* **2013**, *23* (5), 778–87.
- (44) Levene, M. J.; Korlach, J.; Turner, S. W.; Foquet, M.; Craighead, H. G.; Webb, W. W. *Science* **2003**, *299* (5607), 682–6.
- (45) Ibach, J.; Brakmann, S. *Angew. Chem., Int. Ed.* **2009**, *48* (26), 4683–5.
- (46) Eid, J.; Fehr, A.; Gray, J.; Luong, K.; Lyle, J.; Otto, G.; Peluso, P.; Rank, D.; Baybayan, P.; Bettman, B.; Bibillo, A.; Bjornson, K.; Chaudhuri, B.; Christians, F.; Cicero, R.; Clark, S.; Dalal, R.; Dewinter, A.; Dixon, J.; Foquet, M.; Gaertner, A.; Hardenbol, P.; Heiner, C.; Hester, K.; Holden, D.; Kearns, G.; Kong, X.; Kuse, R.; Lacroix, Y.; Lin, S.; Lundquist, P.; Ma, C.; Marks, P.; Maxham, M.; Murphy, D.; Park, I.; Pham, T.; Phillips, M.; Roy, J.; Sebra, R.; Shen, G.; Sorenson, J.; Tomaney, A.; Travers, K.; Trulson, M.; Vieceli, J.; Wegener, J.; Wu, D.; Yang, A.; Zaccarin, D.; Zhao, P.; Zhong, F.; Korlach, J.; Turner, S. *Science* **2009**, *323* (5910), 133–8.
- (47) Samiee, K. T.; Moran-Mirabal, J. M.; Cheung, Y. K.; Craighead, H. G. *Biophys. J.* **2006**, *90* (9), 3288–99.
- (48) Edel, J. B.; Wu, M.; Baird, B.; Craighead, H. G. *Biophys. J.* **2005**, *88* (6), L43–5.
- (49) Korlach, J.; Marks, P. J.; Cicero, R. L.; Gray, J. J.; Murphy, D. L.; Roitman, D. B.; Pham, T. T.; Otto, G. A.; Foquet, M.; Turner, S. W. *Proc. Natl. Acad. Sci. U.S.A.* **2008**, *105* (4), 1176–81.
- (50) Liao, D.; Galajda, P.; Riehn, R.; Illic, R.; Puchalla, J. L.; Yu, H. G.; Craighead, H. G.; Austin, R. H. *Opt. Express* **2008**, *16* (14), 10077.
- (51) Uemura, S.; Aitken, C. E.; Korlach, J.; Flusberg, B. A.; Turner, S. W.; Puglisi, J. D. *Nature* **2010**, *464* (7291), 1012–7.
- (52) Sameshima, T.; Iizuka, R.; Ueno, T.; Wada, J.; Aoki, M.; Shimamoto, N.; Ohdomari, I.; Tanii, T.; Funatsu, T. *J. Biol. Chem.* **2010**, *285* (30), 23159–64.
- (53) Richards, C. I.; Luong, K.; Srinivasan, R.; Turner, S. W.; Dougherty, D. A.; Korlach, J.; Lester, H. A. *Nano Lett.* **2012**, *12* (7), 3690–4.
- (54) Zhao, J.; Branagan, S. P.; Bohn, P. W. *Appl. Spectrosc.* **2012**, *66* (2), 163–9.
- (55) Chen, J.; Petrov, A.; Tsai, A.; O'Leary, S. E.; Puglisi, J. D. *Nat. Struct. Mol. Biol.* **2013**, *20* (6), 718–27.
- (56) Zhao, Y.; Chen, D.; Yue, H.; French, J. B.; Rufo, J.; Benkovic, S. J.; Huang, T. J. *Lab Chip* **2013**, *13* (12), 2183–98.
- (57) Miyake, T.; Tanii, T.; Sonobe, H.; Akahori, R.; Shimamoto, N.; Ueno, T.; Funatsu, T.; Ohdomari, I. *Anal. Chem.* **2008**, *80* (15), 6018–22.
- (58) Teng, C. H.; Lionberger, T. A.; Zhang, J.; Meyhofer, E.; Ku, P. C. *Nanotechnology* **2012**, *23* (45), 455301.
- (59) Kinz-Thompson, C. D.; Palma, M.; Pulukkunat, D. K.; Chenet, D.; Hone, J.; Wind, S. J.; Gonzalez, R. L., Jr. *ACS Nano* **2013**, *7* (9), 8158–8166.
- (60) Lundquist, P. M.; Zhong, C. F.; Zhao, P.; Tomaney, A. B.; Peluso, P. S.; Dixon, J.; Bettman, B.; Lacroix, Y.; Kwo, D. P.; McCullough, E.; Maxham, M.; Hester, K.; McNitt, P.; Grey, D. M.; Henriquez, C.; Foquet, M.; Turner, S. W.; Zaccarin, D. *Opt. Lett.* **2008**, *33* (9), 1026.
- (61) Whitesides, G. M. *Nature* **2006**, *442* (7101), 368–73.
- (62) Zhao, Y.; Stratton, Z. S.; Guo, F.; Lapsley, M. I.; Chan, C. Y.; Lin, S. C.; Huang, T. J. *Lab Chip* **2013**, *13* (1), 17–24.
- (63) Yang, S.; Guo, F.; Kiraly, B.; Mao, X.; Lu, M.; Leong, K. W.; Huang, T. J. *Lab Chip* **2012**, *12* (12), 2097–102.
- (64) Moerner, W. E.; Fromm, D. P. *Rev. Sci. Instrum.* **2003**, *74* (8), 3597.
- (65) Patterson, G. H.; Piston, D. W. *Biophys. J.* **2000**, *78* (4), 2159–2162.
- (66) Benkovic, S. J.; Valentine, A. M.; Salinas, F. *Annu. Rev. Biochem.* **2001**, *70*, 181–208.
- (67) Arumugam, S. R.; Lee, T. H.; Benkovic, S. J. *J. Biol. Chem.* **2009**, *284* (43), 29283–9.
- (68) Delagoutte, E.; von Hippel, P. H. *J. Mol. Biol.* **2005**, *347* (2), 257–75.
- (69) Zhang, Z.; Spiering, M. M.; Trakselis, M. A.; Ishmael, F. T.; Xi, J.; Benkovic, S. J.; Hammes, G. G. *Proc. Natl. Acad. Sci. U.S.A.* **2005**, *102* (9), 3254–9.
- (70) Lefebvre, S. D.; Morrical, S. W. *J. Mol. Biol.* **1997**, *272* (3), 312–26.
- (71) Spiering, M. M.; Nelson, S. W.; Benkovic, S. J. *Mol. Biosyst.* **2008**, *4* (11), 1070–4.
- (72) Perumal, S. K.; Ren, W.; Lee, T. H.; Benkovic, S. J. *Proc. Natl. Acad. Sci. U.S.A.* **2013**, *110* (1), 99–104.
- (73) Lee, W.; Jose, D.; Phelps, C.; Marcus, A. H.; von Hippel, P. H. *Biochemistry* **2013**, *52* (18), 3157–70.
- (74) Perumal, S. K.; Yue, H.; Hu, Z.; Spiering, M. M.; Benkovic, S. J. *Biochim. Biophys. Acta* **2010**, *1804* (5), 1094–112.
- (75) Yang, J.; Trakselis, M. A.; Roccasecca, R. M.; Benkovic, S. J. *J. Biol. Chem.* **2003**, *278* (50), 49828–38.
- (76) Xi, J.; Zhuang, Z.; Zhang, Z.; Selzer, T.; Spiering, M. M.; Hammes, G. G.; Benkovic, S. J. *Biochemistry* **2005**, *44* (7), 2305–18.
- (77) Bleuit, J. S.; Xu, H.; Ma, Y.; Wang, T.; Liu, J.; Morrical, S. W. *Proc. Natl. Acad. Sci. U.S.A.* **2001**, *98* (15), 8298–305.
- (78) Hinerman, J. M.; Dignam, J. D.; Mueser, T. C. *C. J. Biol. Chem.* **2012**, *287* (22), 18608–17.
- (79) Nelson, S. W.; Yang, J.; Benkovic, S. J. *J. Biol. Chem.* **2006**, *281* (13), 8697–706.